Electromagnetic forces in photonic crystals

M. I. Antonoyiannakis* and J. B. Pendry
Condensed Matter Theory Group, The Blackett Laboratory, Imperial College, London SW7 2BZ, United Kingdom
(Received 26 January 1999)

We have developed a general methodology for computing electromagnetic (EM) fields and forces in matter, based on solving the macroscopic Maxwell's equations numerically in real space and adopting the time-averaged Maxwell stress tensor formalism. We can treat both dielectric and metallic systems characterized by a local frequency-dependent dielectric function, and of any size and geometry in principle. In this paper, we are particularly interested in calculating forces on nanostructures, induced by a beam of monochromatic light (such as a laser). The motivation behind this particular direction is the facilitation of self assembly in colloidal systems with the aim of aiding the fabrication of photonic crystals. We first look at two homogeneous systems: a half space and a layer. In passing from a low-ϵ to a high-ϵ medium, the light beam always attracts the interface (i.e., the *surface* force is negative). Thus the surfaces of two liquids separated by a layer of lower ϵ will generally be attracted towards each other, whereas for solids the *total* force must also be negative. This condition is not satisfied for the EM field of a traveling wave, but may be fulfilled for an evanescent wave. Thus, by shining evanescent light in the region between two solid bodies an attraction between them may be induced. We then study the EM forces induced by a laser beam on a three-dimensional crystal of dielectric spheres of GaP in air. At wavelengths comparable to the lattice constant, multiple scattering effects tune in: band gaps, Bragg scattering. But in all these cases the incident beam induces positive pressure on (and between) the spheres. Much more interesting is the regime where the radiation couples to the EM eigenmodes supported by isolated spheres (Mie resonances). These modes are analogous to electronic orbitals and, like their electronic counterparts, can form bonding and antibonding interactions between neighboring spheres. By irradiating the system with light at the bonding frequency an attractive interaction is induced between the spheres. For moderate intensities of the incident radiation these forces can overcome all other interactions present (gravitational, thermal, and Van der Waals) and may provide the main mechanism for formation of stable crystal structures in colloidal systems. [S0163-1829(99)09027-X]

I. INTRODUCTION

A. Photonic structures

The realization that by adjusting the geometric and dielectric parameters of a photonic crystal, we can alter the *optical* properties at will,[1–5] has fuelled prospects for novel optical phenomena (such as photon localization, inhibition of spontaneous emission and enhanced nonlinear effects) and devices [single-mode light-emitting diodes, thresholdless lasers, etc.].

For such novel effects to be observable, one needs photonic crystals of certain crystalline structure, small disorder, and large refractive index contrast. Following intensified efforts over the past years we are now starting to have artificial opals at visible wavelengths, fabricated by a wealth of experimental techniques.[6]

The theoretical understanding of photonic structures has centered at solving Maxwell's equations for the electromagnetic (EM) wave field in the presence of matter. Thus, the classical theory of vector fields is applied. This methodology, appropriate for scales large enough compared to the underlying atomic structure, has been successfully applied to predict both the dispersion relation (band structure) as well as the scattering properties of such systems.

B. Overview of photonic forces

Nature favors phenomena that are energetically profitable. For example, the Van der Waals force between two macroscopic objects can be found by calculating the change in the self energy of the vacuum-fluctuation wave fields, which multiply scatter off the objects. In electronic band structure, total energy calculations combined with variational arguments have been successfully used to predict the equilibrium structure of crystals and to realistically estimate a plethora of physical quantities.[7]

Our involvement with forces is motivated by the current state of affairs in self assembly of colloidal particles. Two major causes for crystallization in these systems are the gravitational and Van der Waals forces. Of these two, gravity leads invariably to close-packed structures, whereas the Van der Waals force favors only one structure at a time. Heating can at most provide a phase transition to another well-defined crystalline structure. But for optimal optical properties in a photonic crystal, it is often necessary to obtain a particular structure that may not happen to be favored by gravity or Van der Waals. We wanted to go a step further by studying first how the crystalline structure affects the EM modes (bands), and then using the knowledge of these modes to affect changes in the structure by inducing systematic attractions/repulsions while also maintaining the stability of the final crystal. Information of the EM-field distribution alone is not enough to answer these questions, as we shall see; hence the need to calculate EM forces.

To give an example, consider what happens to a photonic crystal of dielectric spheres as we traverse with a laser of tunable frequency a resonant mode (these modes are de-

scribed later). At the resonance the fields inside the spheres are enhanced strongly and the corresponding energy density increases by a factor of 1000; away from the resonances the enhancement factor drops to about 5. This shifting of the wave field from one region of the crystal to another strongly affects the forces that result in the subsequent movement of the spheres, and may have important implications and applications in colloidal assemblies.

Apart from performing total energy calculations, EM forces can be also computed in an alternative, more formal manner: namely within the Maxwell Stress Tensor (MST) formalism. In this methodology, the various components of the MST are constructed from the electric and magnetic fields in real space. Integration of the tensor around a closed surface surrounding the body of interest yields the total force acting on it (surface or other local forces may be obtained by integrating around part of the body). There is in principle no restriction as to the size and shape of the body, nor as to its dielectric properties. The generality of this method makes its applicability wide, ranging from purely electric to purely magnetic to fully electromagnetic effects, and from traveling to evanescent wave fields.

Our approach in this paper is as follows: First, we explain in some detail how the concept of a stress tensor arises in the calculation of forces. We define the tensor for the case of electromagnetism and show how it can be incorporated in numerical calculations of photonic effects. We then put our methodology at work. First, we study how traveling and evanescent fields affect the forces between two homogeneous half spaces separated by a surface or a dielectric layer. This is followed by the main body of our results, which regards light-induced forces on three-dimensional (3D) dielectric crystals.

II. METHODOLOGY

A. Theoretical framework

1. The need for a stress tensor

We are interested in calculating EM forces on macroscopic bodies in the nanometer scales. It is therefore natural to seek expressions for the forces in terms of macroscopic quantities (such as dielectric functions). We, therefore, make at the outset an implicit adoption of the continuum picture of matter. We follow the treatment of Landau and Lifshitz.[8]

A force acting on a macroscopic system is a sum of the forces $\mathbf{f}_v(\mathbf{r})$ on each of the volume elements that constitute the system. Thus, the total force $\mathbf{F}$ is

$$\mathbf{F}=\int \mathbf{f}_v(\mathbf{r})\,dv. \tag{1}$$

If $\mathbf{f}_v$ can be expressed as the divergence of a tensor of rank two, then we can transform the volume integral into a surface integral and the total force becomes

$$F_\alpha=\int \frac{\partial \overleftrightarrow{T}_{\alpha\beta}}{\partial x_\beta}dv, \quad \alpha,\beta=\{x,y,z\}, \tag{2}$$

$$= \oint \oint \overleftrightarrow{T}_{\alpha\beta}dS_\beta, \tag{3}$$

where a sum over repeated indices is implied from here onwards. The *stress tensor* $\overleftrightarrow{T}_{\alpha\beta}$ contains all the information we need. Note it has dimensions of energy density. This is not accidental, since forces can be also thought to arise due to changes in the energy under a virtual displacement of the system. Therefore, only the spatially varying part of $\overleftrightarrow{T}_{\alpha\beta}$ contributes to forces, a fact which can be seen in Eq. (2). Equation (3) is of great practical benefit in that it is often easier to calculate the stress tensor on the surface $\mathbf{S}$ enclosing a solid body rather than in its interior.

2. The stress tensor for electromagnetism

So far the discussion is general. For the case of electromagnetism, Eqs. (1)–(3) describe the force transmitted across the surface $\mathbf{S}$ and acting on the *combined* system of particles and fields inside the volume element. From this we can obtain the force on matter alone by subtracting the rate of change of the radiation momentum internal to the volume; however for systems of interest to us this term is zero and therefore of no consequence, as we explain later. Now we need the stress tensor.

When a solid body is immersed in a linear, isotropic medium of permittivity $\epsilon_0\epsilon_m$ and permeability $\mu_0\mu_m$ that do not change with density changes or pure shears, then the spatially nonconstant part of the stress tensor in the region external to the body is given in terms of the electric ($\mathbf{E}$) and magnetic ($\mathbf{H}$) fields by[9]

$$\overleftrightarrow{T}_{\alpha\beta}=\epsilon_0\epsilon_m E_\alpha E_\beta+\mu_0\mu_m H_\alpha H_\beta - \frac{1}{2}\delta_{\alpha\beta}(\epsilon_0\epsilon_m E_\gamma E_\gamma+\mu_0\mu_m H_\gamma H_\gamma) \tag{4}$$

provided the medium remains in mechanical and thermal equilibrium under the influence of the EM fields. Thus, by integrating $\overleftrightarrow{T}_{\alpha\beta}$ of Eq. (4) over a closed surface $\mathbf{S}$ enclosing the system, the *full* EM force on the system is obtained. No further approximations or limiting assumptions need be made, as has often been done with other methodologies employed for EM effects (e.g., dipole approximation, vanishing particle size compared to the wavelength of light in scattering phenomena, etc.). Our methodology can be applied to dielectric or metallic objects of any shape and at any frequency range in principle. The only requirement for meaningful results is that the integration is carried out over scales that are large with respect to atomic sizes, so that the continuum picture of matter is justified. For nanostructure scales of interest to us (>50 nm) this requirement is surely satisfied: the dynamics of the EM wave field is more properly described by the equations of Maxwell rather than by the Schrödinger equation for all the electronic charges that make up the dielectric response of the system. This choice of macroscopic scales dictates a relevant timescale also for the type of fields we are interested in (no macroscopic object can respond synchronously to THz oscillations): we must time average the forces (i.e., the stress tensor) over many cycles when dealing with harmonic fields at optical frequencies. A consequence of time averaging is that the rate of change of the EM-field momentum inside the volume of integration vanishes. Thus, it is the material bodies that absorb all mo-

mentum transfer between our system and the outside world. The stress tensor integration yields exactly this force.

B. Numerical methods

We discretize Maxwell's equations on a simple cubic (SC) mesh. For calculations of photonic band structure, periodic boundary conditions are used in all directions. For transmission results, we consider a crystal finite in the z direction, having a thickness of N unit cells (layers), N being allowed to vary. We shall discuss here the case where a monochromatic light beam of frequency ω, polarization σ and wave vector $\mathbf{k}$ is incident on the crystal from the $-z$ side. Using the transfer-matrix formalism we calculate reflection coefficients $R_{\mathbf{k}'\sigma'}$ for scattering into plane waves of wave vector $\mathbf{k}'=\mathbf{k}_\parallel+\mathbf{g}_\parallel+\hat{\mathbf{z}}k'_z$ and polarization σ', where $\mathbf{k}_\parallel$ is the component of $\mathbf{k}$ parallel to the xy plane and $\mathbf{g}_\parallel$ is a *two-dimensional* reciprocal lattice vector also lying on the xy plane. Our computer codes have been published and issues of stability and accuracy have been discussed elsewhere.[10]

The new ingredient is the calculation of forces. From the reflection coefficients we construct the total fields on the $-z$ side of the crystal,

$$\mathbf{E}(\mathbf{r},t)=\mathbf{E}^0_{inc}\sum_{\mathbf{k}',\sigma'}(\delta_{\mathbf{k}\mathbf{k}'}\delta_{\sigma\sigma'}+R_{\mathbf{k}'\sigma'})\hat{\mathbf{e}}_{\mathbf{k}'\sigma'}e^{i[\mathbf{k}'\cdot\mathbf{r}-\omega t]}, \tag{5a}$$

$$\mathbf{H}(\mathbf{r},t)=\mathbf{H}^0_{inc}\sum_{\mathbf{k}',\sigma'}(\delta_{\mathbf{k}\mathbf{k}'}\delta_{\sigma\sigma'}+R_{\mathbf{k}'\sigma'})\hat{\mathbf{e}}_{\mathbf{k}'\sigma'}e^{i[\mathbf{k}'\cdot\mathbf{r}-\omega t]}. \tag{5b}$$

In Eq. (5) $\mathbf{E}^0_{inc},\mathbf{H}^0_{inc}$ are the amplitudes of the incident fields and $\hat{\mathbf{e}}_{\mathbf{k}'\sigma'}$ are the unit vectors for each $\mathbf{k}'$ and each polarization σ'. The Kronecker delta functions serve as to add the contribution from the incident field, which is present on the $-z$ side, to the reflected field. For the total fields on the $+z$ side the only contribution comes from the transmitted fields.

Having constructed the total fields outside the crystal, we invoke once again the transfer-matrix equations to find the total field at each mesh point inside the structure. When this is accomplished, the stress tensor components are calculated and time averaged. The latter procedure can be made in a standard way since the fields are expressed as sums of plane waves at the same frequency ω. There is one word of caution when we are dealing with resonances, however: in this case the EM energy and the stress tensor vary rapidly in space, and it is important to allow enough mesh points to describe the spatial decay of the associated evanescent wave fields, otherwise the calculation becomes unstable. Finally, the forces are found by integrating the stress tensor over a surface enclosing the body of interest, which can be of arbitrary shape and complexity. In this paper, we present force calculations on isolated spheres, crystal layers, and the entire crystal sample.

III. RESULTS AND DISCUSSION

A. Homogeneous system—traveling waves

In order to understand some of the main qualitative features of light-induced EM forces, as well as to provide a testbed for our numerical methodology, we first solve (analytically and numerically) for two homogeneous systems: a half space and a layer, both extending infinitely in the xy plane (Figs. 1 and 2).

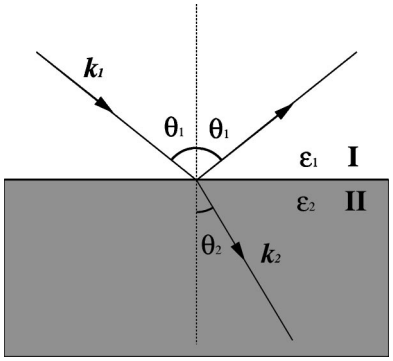

FIG. 1. Reflection and transmission of a beam of monochromatic light upon incidence on the interface between two different semi-infinite dielectric media (half spaces).

The light beam is incident from above and has an infinite cross section, so that edge effects are removed. In practice, a laser beam with a cross section 10 times larger than the area studied suffices for such effects to be avoided, a realistic requirement for modern lasers.

As a dielectric system we chose GaP, which is transparent over near infrared and visible frequencies but has a significant absorption in the ultraviolet spectrum. As a metallic system we use Al, for which the dielectric function can be modeled as

$$\epsilon=1-\frac{\omega_p^2}{\omega(\omega+i\gamma)}, \tag{6}$$

where $\hbar\omega_p=15$ eV and the damping coefficient for the intraband transitions is $\hbar\gamma=0.1$ eV. Our data for the dielectric properties of these materials come from Ref. 11.

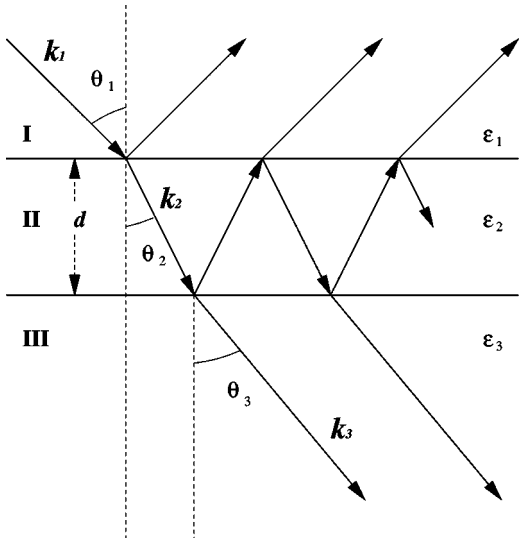

FIG. 2. A wave incident at angle θ_1 from medium I is scattered by the interfaces with media II and III. When $\epsilon_2<\epsilon_1$ the fields in II become evanescent for large enough θ_1. For visual clarity all beams are pictured as rays with zero cross section; in our calculations we regard each beam as having infinite cross section.

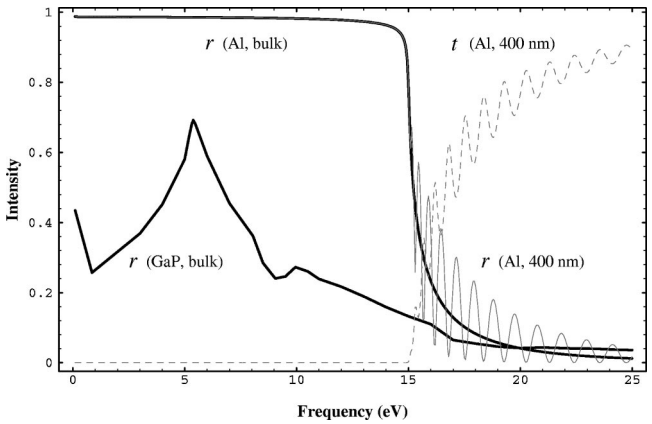

FIG. 3. The intensity of reflected light, at normal incidence, from two semi-infinite homogeneous systems, GaP and Al, is shown in thick lines. The sharp decline in reflectance for Al is due to the plasma frequency $\omega_p = 15$ eV. A finite but substantially thick (400 nm) layer of Al also reflects most light below ω_p; above ω_p it displays a ripple structure due to multiple reflections of the waves from the sides of the layer (Fabry-Perot oscillations). Reflectance (transmittance) for the finite layer is shown in continuous (broken) thin lines.

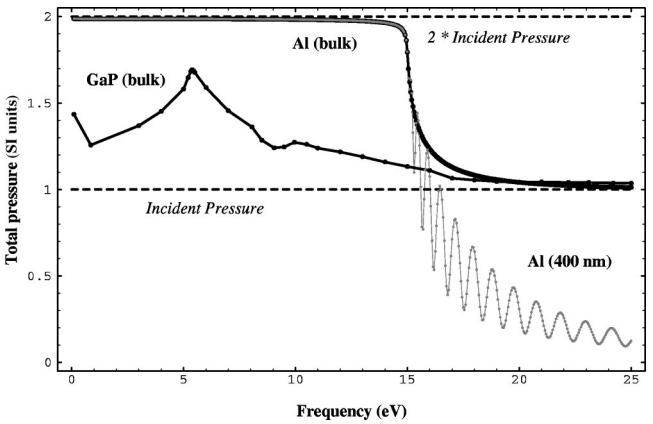

FIG. 4. Total pressure on a homogeneous medium of infinite (GaP and Al half spaces, thick curves) and finite (Al 400 nm, thin curves) thickness. Light is normally incident from air with intensity $I_0 \sim 3\times 10^8$ W/m^2. The incident radiation pressure is $P_{inc} = I_0/c_0 = 1$. Positive values for the pressure imply that the light is pushing the system. (i) For the half spaces, the pressure is calculated with the stress-tensor method analytically (continuous thick lines) and numerically (dotted-thick lines) in perfect agreement. It ranges from P_{inc} (full absorption) to $2P_{inc}$ (full reflection) irrespective of the different dielectric properties of the GaP and Al media. (ii) In contrast, a layer of finite thickness may allow light to pass with transmittance close to unity, in which case it experiences a pressure close to zero. For the layer the pressure is calculated numerically with the stress-tensor method (continuous thin line) and with the energy-gradient method (dotted-thin line).

We summarize our main findings for the forces on these systems.

1. Half space

(a) *Natural limits*. The response to light incident on a homogeneous half space ranges from full absorption (e.g., for a dielectric at the Brewster angle and *p*-polarized light) to full reflection (e.g., for a perfect metal at frequencies below ω_p) In the former case, the momentum exchange between light and the crystal equals the *z* component of the incident momentum, in the latter case it is twice that. Thus, for normal incidence the pressure on the half space will range respectively from P_{inc} (full absorption) to $2P_{inc}$ (full reflection), where $P_{inc} = I_0/c_0$ is the radiation pressure of the incident beam, which has intensity I_0 and travels at the free-space speed c_0. These effects are demonstrated for GaP and Al samples in Figs. 3 and 4 (thick lines). The values P_{inc} and $2P_{inc}$ constitute therefore the *natural limits* for *total* (i.e., external) EM forces on a general dielectric half space due to incidence of a single beam of light.

(b) *Volume forces*. Inside the homogeneous half space there will be no volume force in any direction if there are no losses, since the transmitted light will propagate unimpeded as in free space (although with a different wave velocity). Therefore, the stress tensor will be constant throughout the medium. However, when absorption is present volume forces occur and are accompanied by a continuous decay of the $\overleftrightarrow{T}_{ij}$ components with *z*.

(c) *Origin of surface forces*. Momentum transfer between the incident light and matter can occur due to a scattering or absorption process. Therefore, a surface force must generally exist on dielectric boundaries, since the reflection/transmission process causes the momentum of the incident light to change. This surface force will be accompanied by a discontinuity in one or more stress tensor components across the interface ($\overleftrightarrow{T}_{zz}$ in our case).

(d) *Sign of surface forces*. For $\epsilon_1 < \epsilon_2$ and both *s* and *p* polarizations the normal component of the interface pressure $P_{z,int}$ is always negative and the interface is attracted by the beam, since

$$P_{z,int} \propto (\epsilon_1 - \epsilon_2). \tag{7}$$

We can physically understand this in terms of the spatial distribution of the EM energy. For *s* light all fields are continuous across the interface, except $D_\parallel$, which is higher in medium 2. Hence, at $z = 0$ the energy density in medium 2 is always higher than in medium 1. The total energy is conserved, but the lower wave velocity in medium 2 means that more energy is ''squeezed'' near the interface on the 0^+ side than on the 0^- side. This imbalance in energy density shows up as a negative force. For *p* light the energy-density balance is not straightforward to predict without doing the calculation; but otherwise the same arguments apply. This intuitive energy-gradient argument explains qualitatively the force, but for normal incidence it is quantitatively correct also. We show in Fig. 5 the MST and the energy-gradient calculations for both Al and GaP. The agreement is excellent.

2. Layer

(a) *Natural limits revisited*. If we replace the half space with a layer of finite thickness such that some light is transmitted through the far end, then the lower bound for the force becomes zero, corresponding to full transmission (i.e., zero reflection and zero absorption). This effect is demonstrated for normal incidence on an Al sample of thickness $d = 400$ nm in Figs. 3 and 4 (thin lines).

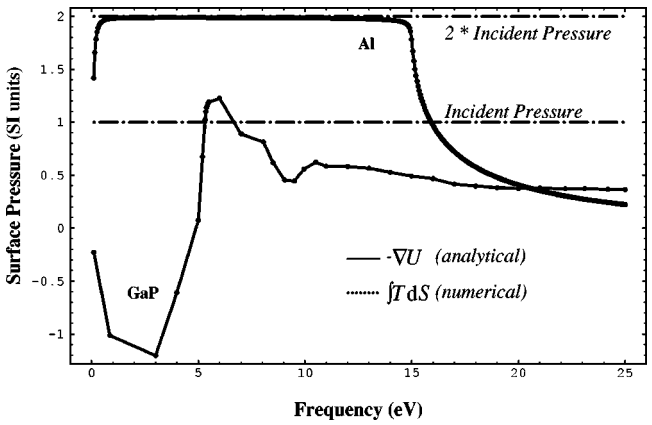

FIG. 5. Light-induced surface pressure on a homogeneous half space (GaP and Al). Normal incidence from air with $I_0 \sim 3\times 10^8$ W/m^2. The pressure is calculated analytically as the differential of the energy density at the interface (i.e., via the energy-gradient method) and is shown in continuous lines; and numerically with the stress-tensor method, shown in dotted lines. There is perfect agreement.

(b) *Interface forces at* $z=d$. With motivation for self assembly, we are interested in producing attractive forces between media I and III. Irrespective of whether the waves are traveling or evanescent, the interface force at $z=d$ is attractive (negative) when $\epsilon_3 > \epsilon_2$. This is satisfied for at least some range of frequencies when II is vacuum and III is a semiconductor/insulator—but not if III is a metal. The same holds true for the interface force at $z=0$: the sign of the force on the interface is given by $(\epsilon_2-\epsilon_1)$. Consequently, any light beam passing through two liquid media separated by a layer of lower ϵ will induce an attraction between the liquid surfaces. If the liquids are incompressible their surfaces will move towards each other. The inverse situation occurs for light falling from air (medium I) onto a liquid layer (medium II): the liquid expands in both interfaces. Such behavior has been described by Kats and Kontorovich[12] in connection with the self focusing of a laser beam in a liquid medium.

(c) *Total forces.* When only traveling waves exist in all three media, the two half spaces repel each other. In this case, the photons can be thought of as tennis balls: as they scatter off the walls of I and II, they exert a positive pressure on each wall.

B. Homogeneous system—evanescent waves

We saw that two solid bodies cannot be attracted towards each other via traveling waves. The situation is different for evanescent wave fields. In such fields the light wave vector $\mathbf{k}$ acquires an imaginary component so that the dispersion relation is always satisfied

$$\epsilon = (c_0/\omega)^2 \mathbf{k}\cdot\mathbf{k} \tag{8}$$

$$= \tilde{\mathbf{k}}\cdot\tilde{\mathbf{k}}, \tag{9}$$

where ϵ is the relative permittivity of the medium of propagation, and the wave vector $\tilde{\mathbf{k}}$ is dimensionless. Equation (9) is practical because we can derive the wave vectors from ϵ (or vice versa) without worrying about units.

In this section, we concentrate on the layer system (see Fig. 2). The layer is denoted as medium II and separates two dielectric half spaces I, III. For simplicity media I and II are assumed absorption free, whereas for medium III we let $\epsilon_3 = \epsilon_3' + i\epsilon_3''$ in order to test how sensitive our results are to some absorption in the system. A beam of light of wavelength λ is incident from medium I, where it travels with speed c_1, at an angle θ_1 and a wave vector $\tilde{\mathbf{k}}_1 = \hat{\mathbf{x}}\tilde{\beta} + \hat{\mathbf{z}}\tilde{\gamma}_1$. Upon penetration into region II, the wave vector may pick up an imaginary component along $\hat{\mathbf{z}}$

$$\epsilon_2 = \tilde{\beta}^2 + \tilde{\gamma}'^2; \quad \tilde{\mathbf{k}}_2 = (\tilde{\beta}, 0, \tilde{\gamma}_2'), \quad \text{when } \tilde{\beta}^2 < \epsilon_2 \tag{10}$$

$$\epsilon_2 = \tilde{\beta}^2 - \tilde{\gamma}''^2; \quad \tilde{\mathbf{k}}_2 = (\tilde{\beta}, 0, i\tilde{\gamma}_2''), \quad \text{when } \tilde{\beta}^2 > \epsilon_2. \tag{11}$$

By choosing $\epsilon_2 < \epsilon_1$ and adjusting θ_1 (since $\tilde{\beta} = \tilde{k}_1 \cos\theta_1$) we can create an evanescent wave in region II with the desirable imaginary momentum $\tilde{\gamma}_2''$. Here, we concentrate on the case of medium II being vacuum ($\epsilon_2 = 1$). We discuss *total* forces on media I and III, not interface forces.

When $\tilde{\mathbf{k}}_2$ has a sufficiently large imaginary component along $\hat{\mathbf{z}}$, the force becomes attractive. In this case the tennis-ball analogy breaks down. Our results indicate that at the electrostatic limit $\lambda \gg d$ the total force on III per unit area varies as

$$P_z = 2\frac{I_0}{c_1}\frac{\tilde{\gamma}_1^2(|\gamma_3|^2 - \gamma_2''^2)}{|\gamma_1' + \gamma_3|^2}. \tag{12}$$

Thus, the force becomes zero when $|\gamma_3| = \gamma_2''$. Curiously, this is the same condition for the angles of refraction θ_2, θ_3 to be equal, since

$$|\tan\theta_i| = \frac{\beta}{|\gamma_i|}, \quad i = \{1,2,3\}. \tag{13}$$

The force is attractive for large angles θ_1, repulsive for small angles. This is seen more clearly for the case of medium III being free of absorption, in which case the formulas simplify to give

$$P_z \sim \begin{cases} (\epsilon_2 - \epsilon_3), & \gamma_3' = 0 \\ \epsilon_3 + \epsilon_2 - 2\epsilon_1 \sin^2\theta_1, & \gamma_3'' = 0. \end{cases} \tag{14}$$

When $\epsilon_1 > \epsilon_3' > \epsilon_2$ and θ_1 increases from 0 the wave field in region II becomes evanescent first; then, at a larger value of θ_1 the wave field in region III becomes evanescent also (*double evanescence*). At this point the force between media I and III becomes attractive and it remains so for all angles greater. On the other hand, for a traveling wave in medium III the force also becomes attractive beyond a threshold for θ_1. So the force is attractive for large enough θ_1.

The magnitude of the attractive force is sensitive to the ratio of the wavelength λ to the layer thickness d over which the evanescent fields decay before entering medium III. We find that for $\lambda/d \sim 5$ the force has already dropped by more than three orders of magnitude compared to its value at the electrostatic limit $\lambda \gg d$. In Fig. 6, we plot the normal pressure P_z versus $\cos\theta_1$ for three cases, (i) $\epsilon_1 < \epsilon_3'$, (ii) $\epsilon_1 = \epsilon_3'$, and (iii) $\epsilon_1 > \epsilon_3'$. For (i) and (ii) the attractive part of

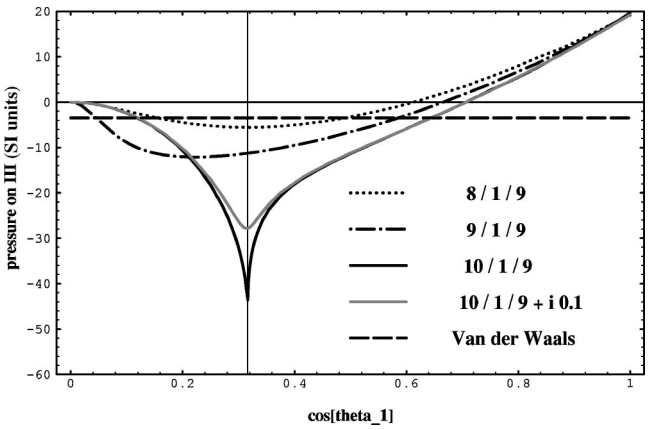

FIG. 6. Total pressure on medium III plotted against the cosine of the angle of incidence, for (i) $\epsilon_1=8$, $\epsilon_2=1$, $\epsilon_3=9$, (ii) $\epsilon_1=9$, $\epsilon_2=1$, $\epsilon_3=9$, and (iii) $\epsilon_1=10$, $\epsilon_2=1$, $\epsilon_3=9$. For system (iii) nonzero absorption ($\epsilon_3''=0.1$) is considered also (grey line). Negative pressure implies attractive force on III. The sharp attraction peak for (iii) occurs when $|\gamma_3|=0$. Zero pressure corresponds to $\gamma_2''=|\gamma_3|$. All curves are for $d=100$ nm, $\lambda/d=100$ and an incident beam intensity $I_0=3.5\times10^9$ W/m^2. The Van der Waals attraction between I and III is smaller than the photoinduced force for most angles; however for light intensities weaker by a factor of 20 or more, or for separations smaller than 50 nm the Van der Waals force dominates all photoinduced effects over all angles.

P_z displays a smooth maximum, whereas for (iii) it peaks sharply. In all cases the highest value of P_z at the electrostatic limit is of the same order of magnitude as the incident radiation pressure I_0/c_1. For (i) and (ii), the field in region III is that of a traveling wave for all angles and therefore $|\gamma_3|>0$. However, for (iii) the field becomes doubly evanescent (in regions II and III) when $\theta_1>\theta_0$, θ_0 being the angle for total internal reflection at an interface between media I and III. This sharp feature in the force persists always at θ_0, provided $\epsilon_1>\epsilon_3'$. Its position in the θ axis is independent of the dielectric properties of layer II. At θ_0 we have $|\gamma_3|=0$. From Eq. (12) it becomes clear why a vanishing γ_3 results into a sharp peak in P_z. For moderate absorption in III, $|\gamma_3|$ does not quite reach zero at θ_0 and the strength of the attraction is reduced although the peak is still clearly seen: for example, the maximum drops by 40% when $\epsilon_3''\sim0.1$. Since the EM force is proportional to the light intensity I_0, we can adjust the latter so that the force induced by the evanescent (or the traveling) wave field supersedes the dispersion forces between the half spaces. We have indicated the strength of the Van der Waals attraction in the figure, calculated in the macroscopic Lifshitz theory with retardation and nonadditivity effects considered. Owing to the d^{-4} behavior of the Van der Waals force,[13] only large enough separations will allow the photoinduced force to dominate.

We conclude that evanescent wave fields may have a role to play in inducing attractive interactions between two dielectric surfaces. The peak at θ_0 for doubly evanescent fields might be of further interest in this direction.

C. Dielectric crystals

We now turn our attention to a 3D crystal of dielectric (GaP) spheres arranged in a SC lattice (Fig. 7). GaP has an

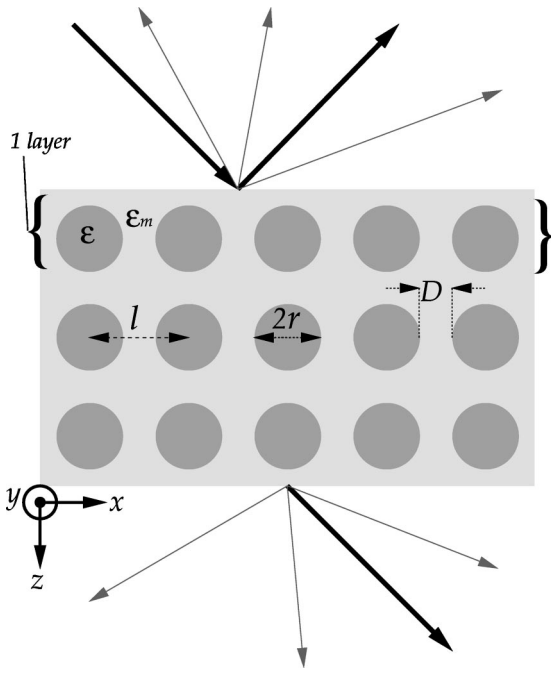

FIG. 7. Our main system of study: A 3D crystal (lattice spacing l) of GaP spheres (r,ϵ) embedded in a medium ϵ_m (usually $\epsilon_m=1$ here). The EM forces are induced by the incidence of one laser beam on the top surface. The crystal responds by reflecting light into the specular beam (thick ray) and under special conditions into the Bragg-reflected beams (thinner rays). Equivalently there is the directly transmitted beam and possible Bragg-transmitted beams. Beams that result from Bragg scattering are also termed ''off-diagonal.'' The crystal is infinite in the xy plane and has thickness N layers (unit cells) in the z direction.

essentially real, constant dielectric function (modeled here as $\epsilon=8.9$) over the frequency range of relevance to this work (0.07–1 eV). The actual absorption of GaP is too small to have any sizeable effect on our force calculations. We consider spheres with a radius $r=200-400$ nm, and choose a lattice spacing $l=900$ nm, so the spherical surfaces are separated by $D=100-500$ nm. We often consider the reference medium in which the spheres are embedded to be air ($\epsilon_m=1$), although, for reasons of experimental feasibility, it is really a liquid medium we have in mind. Such a medium does not alter qualitatively the effects we describe provided its absorption is low enough. For example, we show that water is suitable. The crystal is infinite in the x and y directions, and has thickness N unit cells in the z direction.

For the EM properties of this crystal we expect the following behavior:

(a) Propagation of EM waves in an ''effective medium'' at large wavelengths $\lambda\gg l$ where light senses the crystal as an homogeneous dielectric medium.

(b) Multiple scattering effects: (i) forbidden ranges of frequencies as $\lambda\sim l$ where the multiply scattered waves interfere destructively and annihilate each other inside the crystal; (ii) scattering by specific crystal planes into nonspecular directions as $\lambda^{-1}\sim|\mathbf{k}+\mathbf{G}|/(2\pi)$, $\mathbf{G}$ being a reciprocal lattice vector.

(c) Resonant features at frequencies corresponding to the EM eigenmodes of each sphere.

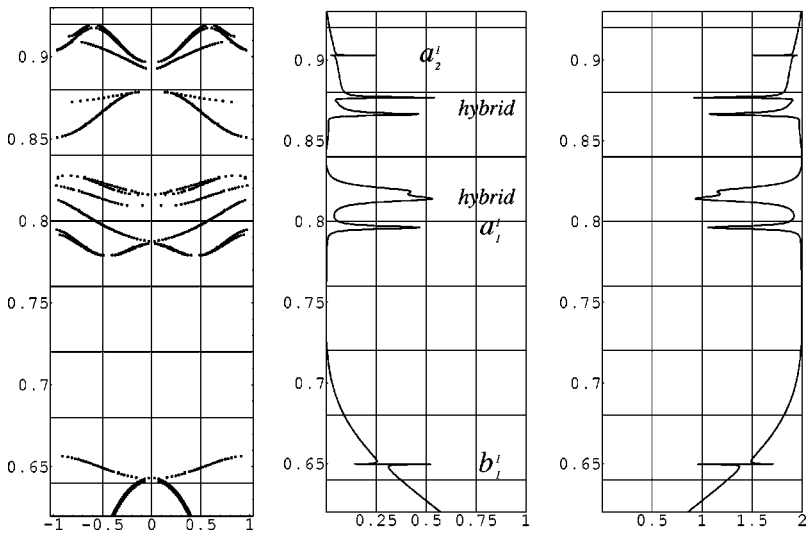

FIG. 8. (a) Photonic band structure along the ΓX direction for a simple cubic lattice of GaP spheres ($r=350$ nm, $\epsilon=8.9$) in air. The vertical axis is in eV units for the frequency and the horizontal axis in in π/l units for the wave vector k_z. (b) Transmittance for a crystal monolayer and for normal incidence along $\hat{\mathbf{z}}$. The sharp peaks correspond in frequency to the low-dispersion modes of the band structure in (b), and occur when the incident light couples to one of the EM eigenmodes of isolated spheres (Mie resonances). Some peaks can be attributed to a single resonance (b_1^1: magnetic dipole mode; a_1^1: electric dipole mode; a_2^1: electric quadrupole mode) while others involve mixing from more than one Mie modes (hybrids) owing to the organization of the spheres in a lattice. (c) Normal pressure (SI units) on one unit cell for the system of (b) and beam intensity $I_0=3\times10^8$ W/m^2. The force scales with I_0.

We observe the effects of (b) and (c) in Fig. 8, where the band structure (dispersion relation) is shown alongside transmittance and force for normal incidence on a crystal monolayer; the effects of (a) appear at lower frequencies not shown in the figure.

Thus, at energies up to at least 0.1 eV, ω is proportional to the wave vector k_z and the constant of proportionality is the wave velocity of a homogeneous effective medium, of dielectric function ϵ_{eff}, replacing the crystal. Within the context of the Garnett theory[14] we find $\epsilon_{eff}=1.76$. At low energies (or wavelengths $\lambda>10\times l$) the force on the crystal is well approximated by the analytical expression for the force on a homogeneous film of the same thickness and dielectric function ϵ_{eff}.

At higher energies band gaps open up and the propagation of all EM modes is forbidden inside an infinite crystal: all incident light will be reflected back when the frequency lies within a band gap. It is impressive that even for one layer of thickness the second band gap centered at around 0.72 eV causes a low transmission. Consequently the pressure on the layer approaches the upper natural limit $2P_{inc}$ for frequencies inside this gap. The first band gap [centered at 0.47 eV, not shown in Fig. 8(a)] requires a thicker sample before it can clearly show its signature in transmission and force spectra, but otherwise it affects the system's behavior in the same way.

The first gap is clearly a lattice effect. It forms at energies near the first crossing of 4 bands (two for each polarization) at the edge of the first Brillouin zone. The second gap, however, is associated with the onset of the resonance at 0.65 eV, which is a *single-sphere* effect and is present for any thickness; hence this gap affects the transmittance spectrum even for one layer of thickness.

Another consequence of multiple scattering is that under certain conditions, the scattered fields can interfere constructively and produce outgoing waves in additional directions to those of the specularly reflected and directly transmitted beams. We call this scattering *off-diagonal*, since when it occurs the wave vector of the scattered field picks up a 2D reciprocal lattice vector component,

$$\mathbf{k}'=\mathbf{k}_\parallel+\mathbf{g}_\parallel+\hat{\mathbf{z}}k_z', \tag{15}$$

whereas the energy conservation requests that

$$k'=k. \tag{16}$$

Most often the energetics of the problem is such that k_z' is imaginary and all the off-diagonal fields are evanescent. However, at certain ranges of frequencies a real k_z' is allowed from Eq. (16) and the off-diagonally scattered beams are traveling waves. For a SC lattice the minimum energy for this to occur is for the smallest possible but nonzero $\mathbf{g}_\parallel$ i.e., when $\mathbf{k}_\parallel$ lies at the edge of the first Brillouin zone along the ΓX direction. Considering an incident beam with $\mathbf{k}=(k_x,0,k_z)$, the condition for nonzero $\mathbf{g}_\parallel$ and real k_z' becomes

TABLE I. Mie modes of an isolated GaP sphere ($\epsilon=8.9$) and their corresponding *order parameter* (mode frequency times sphere radius) in units of eV×nm. b_n^i (a_n^i) modes represent magnetic (electric) multipoles oscillating at the light frequency.

b_1^1	a_1^1	b_2^1	a_2^1	b_3^1	a_3^1	b_1^2	a_1^2	b_4^1	a_4^1	b_2^2	b_5^1
187	214	267	313	346	405	405	410	423	491	493	499

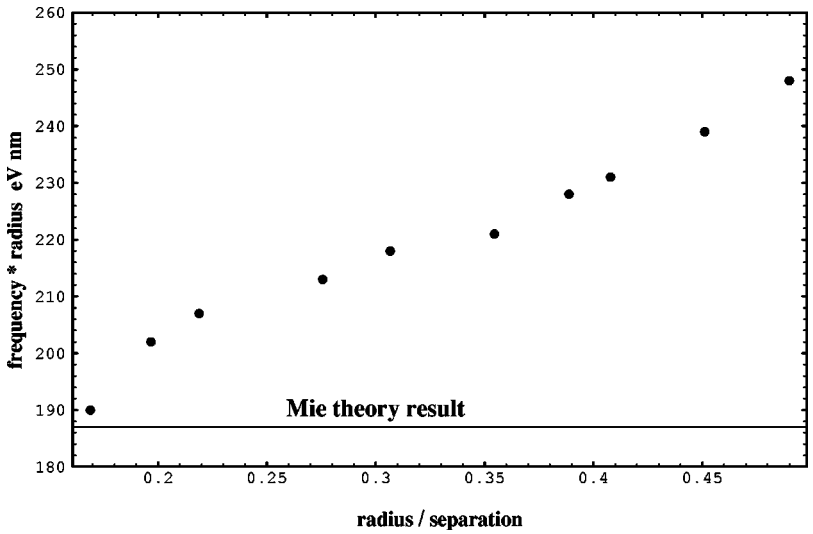

FIG. 9. For a given Mie mode (at frequency ω) of an isolated sphere (radius r), the order parameter $\omega \cdot r$ is independent of the sphere size. When the spheres are put together in a lattice, interactions shift the resonances. When the radius is small compared to the separation (i.e., the unit-cell length l), the one-sphere result is recovered. Results here are for the b_1^1 mode.

$$k \sin\theta = \frac{\pi}{l} \Rightarrow \omega = \frac{\pi}{l} \frac{c_0}{\sin\theta}. \tag{17}$$

Equation (17) gives the lowest frequency for off-diagonal scattering for a SC crystal of lattice constant l and a wave incident from air at an angle θ. For example, for incidence on a crystal monolayer of GaP spheres at $\theta = 70$ deg, off-diagonal scattering sets in at 0.71 eV, in good agreement with Eq. (17). As the frequency increases there are more off-diagonal beams of real momentum generated by the scattering process and the force spectra may become quite complicated.

But clearly the most noteworthy issue is the appearance of resonant forces [for example at 0.65, 0.796, 0.814, 0.866, 0.877, and 0.903 eV in Fig. 8(c)] combined with modes of low dispersion in the band structure. These resonances interest us because firstly, they involve strong forces and secondly, they lead to attractive interactions between the spheres as we shall see.

As regards the strength of the photo-induced force, this is proportional to I_0, the intensity of the incident beam. For a moderate laser of $I_0 \sim 3.5 \times 10^8$ W/m^2 the radiation pressure of the incident beam is $I_0/c_0 \sim 1$ pN per unit cell (of surface area 900×900 nm^2). The *total* force on the crystal may not exceed the natural limit of $2P_{inc} \sim 2$ pN, and in resonances it varies typically between 1 and 2 pN. However when more than one crystal layers are put together then the light-induced resonant interactions *between* the layers (i.e., the total forces on individual spheres) may easily be enhanced to 10 times or more the incident radiation pressure (e.g., 8 pN at 1.08 eV of Fig. 10). By contrast, the gravitational force on a GaP sphere is $mg \sim 0.8 \times 10^{-3}$ pN. Thermal-fluctuation forces are com-

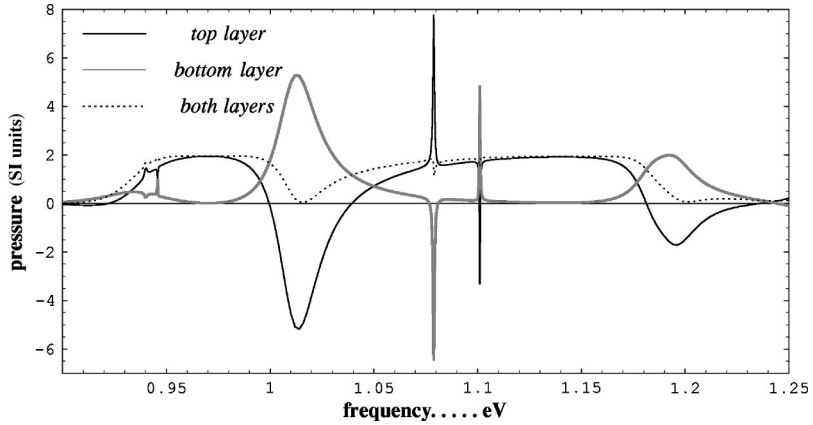

FIG. 10. Normal pressure on a two-layer crystal of GaP spheres ($\epsilon = 8.9$, radius $r = 220$ nm, $f = 0.06$) in air when light is incident normally with intensity $I_0 = 3 \times 10^8$ W/m^2. The pressure on the top (bottom) layer is shown in a thin black (thick grey) line; on both layers (i.e., total pressure) it is shown in a dotted line. At resonant frequencies the forces on either layer are generally opposite in direction, peak sharply and their sign alternates with frequency, exhibiting a series of bonding/antibonding interactions (i.e., layers attract/repel each other). At the bonding modes the spheres of the two layers behave as oscillating EM multipoles oriented parallel to each other, at the antibonding modes they are antiparallel. Here the magnetic dipole (b_1^1) modes are seen at $\sim$0.94 eV, and the electric dipole (a_1^1) modes at 1.08 and 1.1 eV. The broad peaks of repulsion (at 1.01 and 1.2 eV) have nonresonant origins, owing to the multiple scattering of photons between the layers. The strength of the resonant forces is enhanced with increasing f. The pressure is in SI units.

parable to gravity. Finally, the Van der Waals attraction between two GaP spheres at these distances is less than 0.2 pN.[16] Thus provided the spheres are in a liquid medium that facilitates heat evacuation (so that melting is avoided), the photo-induced resonant force can dominate gravitational, thermal-fluctuation and Van der Waals forces.

As regards the nature of the resonant modes, it has been argued elsewhere[15–17] that they correspond to the EM eigenmodes of isolated spheres (*Mie resonances*). Due to the organization of the spheres in a lattice, they acquire a finite but low dispersion (i.e., a low group velocity $d\omega/dk$) and are therefore termed ''heavy photons.''[15] Their presence strongly affects the position of the band gaps on the frequency axis.[18] The eigenmodes are spherical waves labeled by three quantum numbers, just as in the case of electronic orbitals in atoms, and are generally electric or magnetic oscillating multipoles. The analogy to atomic physics is far reaching, as we show below. The notation for the *excitable* electric (magnetic) modes by a plane wave is $a_n^i(b_n^i)$, n being the azimuthal quantum number and i being the sequential index of the resonance in the frequency axis. For dielectric spheres the electric modes a_n^i are broader whereas the magnetic modes b_n^i are sharper, the sharpness of both types of modes increasing with frequency. For metallic spheres, only the electric modes survive, being better known to some as ''surface plasmons.'' The first few Mie resonances for a GaP sphere subjected to a plane wave are shown in Table I.

When many spheres approach to form the infinite crystal, interactions occur which shift the resonances with respect to the frequencies for an isolated sphere (Fig. 9). Unless the coupling between neighboring spheres is strong, each resonance in the crystal will retain its characteristic EM-field distributions on the surface and on the interior of each sphere. Thus we have established that the sharp force feature at 0.65 eV in Fig. 8(c) is a magnetic dipole b_1^1 mode, at 0.796 eV an electric dipole a_1^1, at 0.903 eV an electric quadrupole a_2^1. The EM-field distributions for these three resonances identify completely with the expected patterns for Mie scattering from a single sphere.[18] The three peaks inbetween are hybrids that result from mixing from more than one Mie modes owing to the organization of the spheres into a lattice: at 0.814 eV the fields display a partial similarity to the magnetic quadrupole mode b_2^1 distributions, at 0.866 and 0.877 eV there is partial similarity to the mode a_2^1.

The analogy between the EM eigenmodes of a sphere and the electronic orbitals of an atom leads us to expect an equivalent situation to the degeneracy splitting in atoms, namely that two oscillating multipoles (GaP spheres in a heavy-photon mode) brought close together will interact, their fields will hybridize and the two new energy levels of the combined system would lie slightly below (at $\omega_<$) and slightly above (at $\omega_>$) the frequency of the original level (at ω_0). The mode at $\omega_<$ would identify as bonding (spheres attract each other) whereas at $\omega_>$ as antibonding (spheres repel each other). Such is indeed the case, as we discover when we bring two crystal monolayers in proximity and monitor the forces on the spheres of each layer (top and bottom) induced by a normally incident laser beam, shown in Fig. 10 for spheres of $r=220$ nm. The number of sharp features doubles, as the number of layers does. The forces

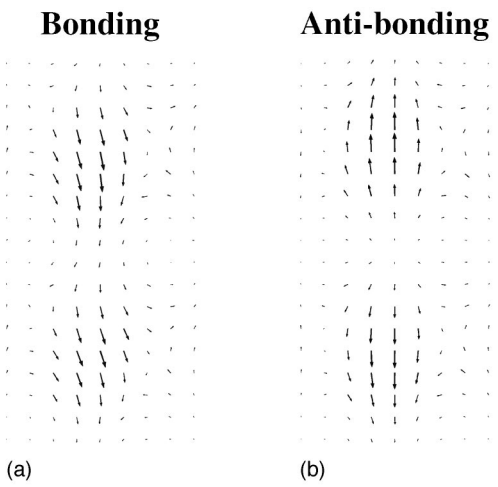

FIG. 11. Bonding and antibonding for the magnetic dipole mode b_1^1 of the two-layer crystal. The **H** field is shown on the cross section xz through the center of two vertically adjacent spheres. Light is s polarized, normally incident from the z direction at the bonding frequency in part (a) (dipoles parallel), at the antibonding frequency in part (b) (dipoles antiparallel). For p polarization the directions of the fields are reversed.

induced on the top and bottom spheres alternate in sign as different resonances are encountered. For the magnetic dipole (b_1^1) mode in particular, we have shown[17] that at $\omega_<$ all spheres have their dipoles parallel and there is attraction between the two layers; whereas at $\omega_>$ the dipoles of the top layer are antiparallel to those of the bottom layer and repel them. The same is true for the electric dipole (a_1^1) mode: all dipoles are parallel at $\omega=1.08$ eV (attraction), antiparallel at $\omega=1.1$ (repulsion) for the system of Fig. 10. Similarly, the multipoles of the higher-energy modes can be oriented constructively, in which case an attraction occurs, or destructively, leading to repulsion between neighboring spheres. This argument holds also for the mixed hybrid states that are made out of more than one Mie modes. Some characteristic EM-field distributions for these cases of bonding and antibonding of dipolar, quadrupolar, and hybrid modes appear in Figs. 11, 12, and 13. To complete the analogy, the splitting of the energy levels and the force strength increase as the spheres of two vertically adjacent layers approach each other (Fig. 14). Thus the potential well (barrier) for attraction (repulsion) becomes deeper (higher) with proximity. The reason for this is that at resonance there are strong evanescent fields induced: the EM-energy density inside each sphere is enhanced up to 3 orders of magnitude compared with the density of the incident beam. At large distances these fields decay to zero and do not give rise to forces, but when another sphere exists nearby they may couple to it and produce a sizeable effect on the force, in a similar manner to what we found for the force between two half spaces separated by a layer of air upon the incidence of evanescent waves.

Incidentally, the broad features around 1.01 and 1.2 eV in the forces on each layer of Fig. 10 are *not* resonances. They form as photons scatter multiply between the layers, banging as tennis balls against each layer and exiting on the lower side eventually with a unit transmittance. Hence, they cause repulsion between the layers, although the total force on the

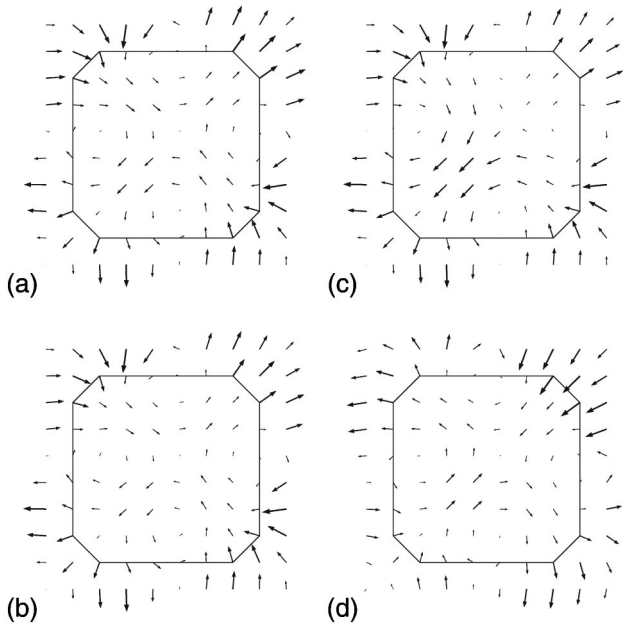

FIG. 12. Bonding and antibonding for the electric quadrupole mode a_2^1 of the two-layer crystal. In all parts the **E** field is shown on the cross section xy through the centre of each sphere. (a) and (b) Top and bottom spheres, bonding mode. (c) and (d) Top and bottom spheres, antibonding mode. At the bonding mode the quadrupoles of the top and bottom spheres are ''parallel,'' at the antibonding mode ''antiparallel.'' The boundaries of the dielectric object (mimicking a sphere) inside the unit cell are drawn for clarity.

crystal is zero. Being interference and not resonance peaks they are rather resistant to absorption: they survive to 60% of their strength when $\epsilon''=0.1$.

The rest of the force spectrum displays mostly smooth, attractive interactions due to the band gaps between the heavy-photon bands. This off-resonance attraction is produced as the band-gap condition for high reflectivity causes

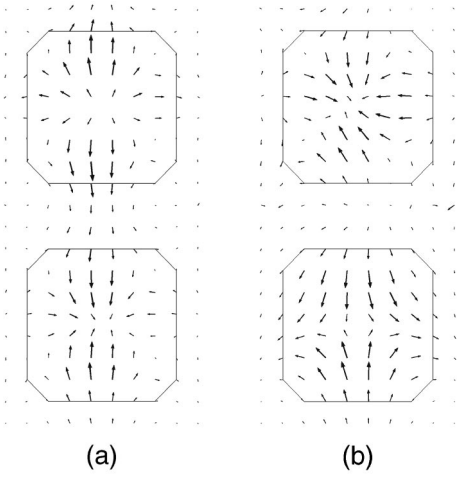

FIG. 13. Bonding and antibonding for a hybrid mode of the two-layer crystal. The **H** field is shown on the cross section xz through the centre of two vertically adjacent spheres. Light is normally incident from the z direction. (a) Bonding frequency, s polarization: constructive alignment of the fields in the two spheres. (b) Antibonding frequency, p polarization: denstructive alignment of the fields.

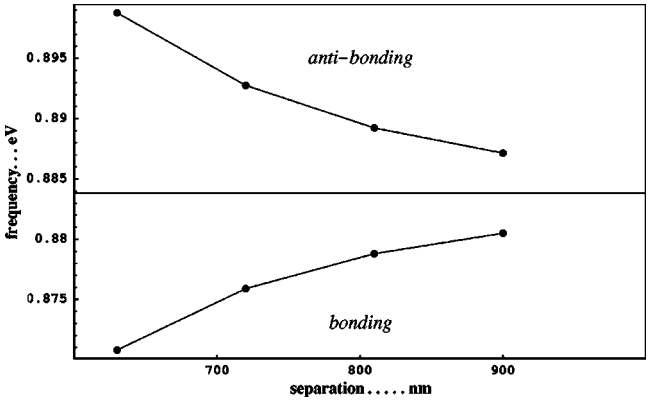

FIG. 14. Resonant energies of a two-layer crystal for normal incidence along $\hat{\mathbf{z}}$ and for the magnetic dipole mode. As the two crystal layers approach each other the bonding/antibonding energy levels of the Mie modes on the spheres split further. The dots denote the energies of the bonding and antibonding modes as a function of the distance of the layers. The spheres have radius $r=240$ nm.

the top layer to absorb almost all the shock from the reflection of the incident light and be therefore pushed towards the bottom layer, which remains relatively inert.

The ability to induce resonant interactions between the spheres of a photonic crystal by shining laser light suggests a possible application in self assembly: by selectively populating the bonding mode we may be able to induce attraction between colloidal particles and promote crystallization into structures that satisfy our purposes even though they may not be favored by gravity or Van der Waals forces. Our calculations may be relevant in one more manner: given the ease with which a two-dimensional photonic crystal is available today, and the relevant difficulty in extending to the third dimension, we suggest that different crystal layers may be attracted and stacked together in a systematic and reversible way by photoinducing the bonding and antibonding forces at will. The generality of the bonding phenomenon adds to this conjecture: all objects support their own Mie-like resonances leading to attraction, no matter how complex their geometry and dielectric function. The angle at which light is incident shifts slightly their frequency but does not suppress the bonding modes. But absorption present in the spheres or the surrounding medium may mask the resonances: a moderate $\epsilon''=0.1$ is enough to suppress them. For GaP spheres in water, however, we have found that the absorption is too small to blur the sharp features in forces, within the frequency range of interest. Also, we have checked that the resonances survive a polydispersion of at least a few percent.

The analogy between resonant, light-induced, sphere-sphere interactions and the bonding of atoms that we just described is not the only one to be made. An analogy exists also with the case of cutting a metal in two along a plane, whereby the bulk plasmons reorganize into surface plasmons of attractive and repelling nature at frequencies below and above the original frequency.[19] The similarities between these three very different systems prompt us to acknowledge a general tendency in nature for the formation of energetically favorable EM bonds between two systems in the same state that come into proximity.

The bond-formation idea extends the Mie scattering

theory of a single sphere since it involves sphere-sphere interactions induced by laser light in a manner that would seem surprising had it not been for our comparison with atomic physics. Furthermore, the Mie theory EM-field distributions may apply to isolated spheres or spheroids; but they become irrelevant for artificial atoms of cubical, rodlike, or more complex shapes that are often used in photonic crystals. Nor may the bonding/antibonding mechanism be guessed by investigating the photonic band structure, since the latter applies to an already built infinite crystal and does not show us the relevant physics as the spheres are gradually brought into proximity. Transmission studies for a crystal two-layers thick do hint at the bonding mechanism, since there appear two peaks in transmittance, but it may not be known positively which of the two peaks leads to attraction, if at all, unless the atomic physics analogy were to be postulated *a priori*, and that would be a bold step! This holds especially for frequency ranges above the electric dipole mode where the modal density is high. Finally, maps of the EM-field distributions on the artificial atoms in photonic crystals may demonstrate bonding/antibonding effects. However, they do not tell us the strength of the interaction and are highly uneconomical in terms of the amount of data stored. Besides, for modes of $n>2$ or for mixed modes the distributions become complicated, and it gets difficult to guess whether there is attraction or repulsion between the layers.

Furthermore, the existence and/or the relevance (i.e., the strength) of the nonresonant repeling forces when the photons multiply scatter between the layers, would go unnoticed in transmission spectra, since this effect is associated with unit transmittance (see the broad peaks at 1.01 and 1.2 eV in Fig. 10).

In contrast, our force calculations are advantageous since they always provide a clear and economical answer as to the strength and the attracting/repelling nature of the interactions. Also, local stresses and surface forces may be computed readily and accurately, whereas knowledge of the EM-field distributions might only provide a crude guess as to these questions. Furthermore, with the MST approach we may assess forces along nontrivial (e.g., off normal) directions, as is needed (i) to determine equilibrium structures; (ii) when dealing with the incidence of more than one beam or with off diagonally scattered beams; (iii) for oblique incidence; (iv) for crystals with polyatomic unit cells of low symmetry. And finally, our methodology for monochromatic light may be generalized to all frequencies and include therefore the vacuum-fluctuation modes, allowing for Van der Waals calculations.

The occurrence of resonant bonding effects between spheres may add to the current methods for engineering 3D photonic crystals out of assemblies of colloidal spheres in liquid solutions. Experiments on gold nanospheres (radius $r \sim 10$ nm) by Kimura have shown fast formation of aggregates upon illumination at the surface-plasmon frequency (i.e., the electric-dipole mode a_1^1), in agreement with calculations of the photo-induced Van der Waals dipole-dipole interaction.[20] Burns, Fournier, and Golovchenko on the other hand have concentrated on dielectric microspheres ($r \sim 700$ nm).[21] They have experimentally demonstrated the presence of long-range attractive forces, induced by laser light, between two polystyrene spheres in water. They argue that these are magnetic-dipole interactions, owing their existence to induced currents on the spheres. They calculate the interaction energy between two magnetic dipoles based on a simplified model that works in the long-distance limit $R \gg \lambda$, where R the distance between the dipoles and λ the wavelength of light. From the perspective of Mie resonances this approach is justified because although the spheres Burns *et al.* use possess many different resonances at or near the frequency of their laser light, the large intersphere distance ensures that the dipole approximation works to leading order. Also the electric-dipole solutions are of secondary importance since they are damped compared to the magnetic dipoles.

In contrast to the work of Kimura (metallic spheres) and that of Burns *et al.* ($R \gg \lambda$), we are dealing with *dielectric* spheres at *close proximity* ($R \sim \lambda$). In general, the sphere-sphere interactions in our system display a *mixing* of EM-multipole behavior, unless a specific condition for an isolated Mie resonance is met. For example two spheres of $r = 350$ nm at distances $l = 900$ nm interact at ~ 0.65 eV as oscillating magnetic dipoles, at ~ 0.80 eV as oscillating electric dipoles, at 0.90 eV as oscillating electric quadrupoles and so on. Although the model of Burns, Fournier, and Golovchenko does not apply to our system (due to the close proximity between the spheres), we believe that their physical explanation for the spatially oscillatory shear forces is basically correct: the oscillation is due to the changes in the phase shifts associated with retardation between spheres of different layers.

IV. CONCLUSION

In conclusion, we have presented a general methodology for accurate and efficient computation of time-averaged EM forces in macroscopic matter. Our goal has been to understand light-induced forces in photonic crystals, with a view to self-assembly, cohesion, and stability of colloidal systems.

We study first the EM forces induced by a monochromatic light beam on homogeneous systems such as a half space and a slab. Traveling waves always produce positive total pressure. Evanescent waves, however, may under specific conditions induce attraction between two surfaces, with a force strength even greater than the Van der Waals attraction between them. Evanescent waves look promising therefore in the application to cohesive forces in nanostructures.

Next, we study the forces induced by a laser beam of intensity I_0 on a 3D dielectric crystal of GaP spheres suspended in air in a SC lattice. After identifying the effects of multiple scattering (band gaps and Bragg scattering), we concentrate on the strong-resonant effects at frequencies corresponding to the EM eigenmodes of isolated spheres (Mie resonances). At such frequencies, the spheres behave as oscillating electric or magnetic multipoles drawing up energy from the light and enhancing their internal fields dramatically. An analogy to atomic physics proves far reaching as these resonant modes arrange into bonding and antibonding states as the spheres come together in the lattice, causing highly attractive and repelling interactions which may become dominant over gravitational, thermal, and Van der Waals forces, for large enough (but realistic) values of I_0. The resonant forces survive the finite absorption of a more

realistic reference medium such as water, as well as a polydispersion in the spheres of a few percent. We believe the photoinduced forces therefore to be experimentally observable and relevant to the formation of stable crystals of colloidal nanospheres. Apart from possible applications in the fabrication of 3D photonic crystals, the resonant mechanism leading to the bonding/antibonding effect may contribute to our understanding of novel nonlinear phenomena arising due to the application of laser-light fields in nanostructures.

Note added: After this manuscript had been submitted for publication, Bayer *et al.* reported on the optical modes of coupled photonic molecules.[22] Their experimental evidence strongly supports the bonding/antibonding mechanism suggested by our calculations.

ACKNOWLEDGMENTS

We would like to express our thanks to F.-J. Garcia-Vidal for valuable discussions and comments. M.I.A. would like to acknowledge the Trustees for the Beit Fellowship for Scientific Research for financial assistance.

*Electronic address: manolis@ic.ac.uk

[1] *Photonic Band Gaps and Localization, Nato ARW*, edited by C. M. Soukoulis (Plenum Press, New York, 1993).

[2] *Photonic Band Gap Materials*, Vol. 315 of *NATO Advanced Studies Institute, Series E: Applied Sciences*, edited by C. M. Soukoulis (Kluwer, Dordrecht, The Netherlands, 1996).

[3] J. D. Joannopoulos, R. D. Meade, and J. N. Winn, *Photonic Crystals* (Princeton University Press, Princeton, NJ, 1995).

[4] J. Opt. Soc. Am. B **10** (1993), special issue on developing and applications of materials exhibiting photonic bandgaps, edited by C. M. Bowden, J. P. Dowling, and H. O. Everitt.

[5] J. Mod. Optics **41** (1993), special issue on photonic band structures, edited by G. Kwizki and J. W. Haus.

[6] A list *indicative* of the recent experimental efforts in fabricating photonic crystals follows: G. Feiertag, W. Ehrfeld, H. Freimuth, H. Kolle, H. Lehr, M. Schmidt, M. M. Sigalas, C. M. Soukoulis, G. Kiriakidis, T. Pedersen, J. Kuhl, and W. Koenig, Appl. Phys. Lett. **71**, 1441 (1997); R. D. Pradhan, J. A. Bloodgood, and G. H. Watson, Phys. Rev. B **55**, 9503 (1997); K. A. McIntosh, L. J. Mahoney, K. M. Molvar, O. B. McMahon, S. Verghese, M. Rothschild, and E. R. Brown, Appl. Phys. Lett. **70**, 2937 (1997); S. Noda, N. Yamamoto, and A. Sasaki, Jpn. J. Appl. Phys., Part 2 **35**, L909 (1996); G. Decher, Science **277**, 1232 (1997), and references therein; S-R. Chen, J. A. Kornfield, S. D. Smith, J. T. Grothaus, and M. M. Satkowski, *ibid.* **277**, 1248 (1997), and references therein; W. Shenton, D. Pum, U. B. Sleytr, and S. Mann, Nature (London) **389**, 585 (1997), and references therein; also see references in Ref. 17.

[7] M. C. Payne, M. P. Teter, D. C. Allan, T. A. Arias, and J. D. Joannopoulos, Rev. Mod. Phys. **64**, 1045 (1992).

[8] L. D. Landau and E. M. Lifshitz, *Theory of Elasticity* (Pergamon Press, New York, 1975), Sec. 2.

[9] L. D. Landau and E. M. Lifshitz, *Electrodynamics of Continuous Media* (Pergamon Press, New York, 1960), Secs. 15, 34, and 56.

[10] J. B. Pendry, in Ref. 6, p. 209; P. M. Bell, J. B. Pendry, L. Martín-Moreno, and A. Ward, Comput. Phys. Commun. **85**, 306 (1995); J. B. Pendry and P. M. Bell, in *Photonic Band Gap Materials* (Ref. 3), p. 203.

[11] *Handbook of Optical Constants of Solids*, edited by E. D. Palik (Academic Press, New York, 1985), Part I, p. 369 and Part II, p. 445.

[12] A. V. Kats and V. M. Kontorovich, Zh. Éksp. Teor. Fiz., Pis'ma Red. **9**, 192 (1969) [JETP Lett. **9**, 112 (1969)].

[13] J. N. Israelachvili and D. Tabor, Prog. Surf. Membr. Sci. **7**, 1 (1973).

[14] J. C. Maxwell Garnett, Philos. Trans. R. Soc. London, Ser. A **203**, 385 (1904); **205**, 237 (1906).

[15] K. Ohtaka and Y. Tanabe, J. Phys. Soc. Jpn. **65**, 2265 (1996); **65**, 2276 (1996).

[16] M. I. Antonoyiannakis and J. B. Pendry, Europhys. Lett. **40**, 613 (1997).

[17] M. I. Antonoyiannakis, Ph.D. thesis, Imperial College, 1998.

[18] E. N. Economou and A. Zdetsis, Phys. Rev. B **40**, 1334 (1989); S. Datta, C. T. Chan, K. M. Ho, C. M. Soukoulis, and E. N. Economou, in *Photonic Band Gaps and Localization* (Ref. 2), p. 289.

[19] J. Schmit and A. A. Lucas, Collect. Phenom. **1**, 127 (1973).

[20] K. Kimura, Surf. Rev. Lett. **3**, 1219 (1996).

[21] M. Burns, J.-M. Fournier, and J. A. Golovchenko, Phys. Rev. Lett. **63**, 1233 (1989); Science **249**, 749 (1990).

[22] M. Bayer, T. Gutbrod, J. P. Reithmaier, A. Forchel, T. L. Reinecke, P. A. Knipp, A. A. Dremin, and V. D. Kulakovskii, Phys. Rev. Lett. **81**, 2582 (1998).